

Physical Origin of the Universal Three-body Parameter in Atomic Efimov Physics

Pascal Naidon¹, Shimpei Endo², and Masahito Ueda²

¹*RIKEN Nishina Centre, RIKEN, Wakō 351-0198, Japan, and*

²*Department of Physics, University of Tokyo, 7-3-1 Hongō, Bunkyo-ku, Tōkyō 113-0033, Japan*

(Dated: October 22, 2021)

We address the microscopic origin of the universal three-body parameter that fixes the spectrum of three-atom systems in the Efimov regime. We identify it with the van der Waals two-body correlation, which causes the three-atom system to deform when the three atoms come within the distance of the van der Waals length, effectively preventing them from coming closer due to the kinetic-energy cost associated with this three-body deformation. This deformation mechanism explains the universal ratio of the scattering length at the triatomic resonance to the van der Waals length observed in several experiments and confirmed by numerical calculations.

I. INTRODUCTION

In recent years, the investigation of Efimov physics [1, 2], the universal physics of few particles interacting via nearly resonant short-range interactions, has developed tremendously, both on the experimental [2–22] and theoretical fronts [23–27]. The essence of this physics is the appearance of a universal $1/R^2$ attraction between three particles at an average separation R . This long-range three-body attraction, discovered by V. Efimov [1], emerges from the pairwise interactions, despite their finite range. It can be interpreted as an interaction between two particles mediated by a third particle. Its strength is universally determined by the masses and quantum statistics of the particles. The Efimov attraction extends from distances on the order of the range of the interaction b to distances on the order of $|a|$, where a is the scattering length of the pairwise interaction. It therefore requires $|a| > b$, a condition well satisfied for resonant pairwise interactions. At the unitarity limit $a \rightarrow \infty$, the Efimov attraction extends to infinity. Decaying as $1/R^2$, it supports an infinite number of bound states known as the Efimov trimers. Furthermore, each bound state is related to the neighbouring state by a scale transformation, due to the scale invariance of $1/R^2$ potentials [1, 24], so that the energy spectrum forms a geometric series. This constitutes the most remarkable and characteristic feature of the Efimov trimers. However, since the three particles are attracted to each other, the physics at short separations comparable to the range b fixes the wave functions and spectrum of the Efimov trimers.

Until recently, little had been known about this short-distance physics. Efimov’s original investigation made use of the asymptotic two-body behaviour (or the zero-range potential limit) to derive the three-body attraction, but did not address the short-distance region directly. Its effect on the longer-distance region was accounted for by a three-body boundary condition, expressed either as a phase in the three-body wave function or a log-periodic inverse length Λ known as the Efimov three-body parameter [1]. This long-distance picture is equivalent to a zero-range low-energy picture, where Λ plays the role of

the parameter that renormalises the low-energy effective field theory [26]. The Efimov effect is the only known physical example of the renormalisation-group limit cycle [28]. Since the short-distance region involves the short-range details of the interaction potentials, Λ has long been thought to be a non-universal quantity that is strongly dependent on the individual properties of the system.

Later, it was found that Λ is universally determined in cases where a length scale larger than b arises in the problem, most notably in the case of a narrow Feshbach resonance in the pairwise interaction [29], which entails a large and negative effective range setting the value of Λ [23], and the case of particles with additional dipolar interactions, whose strength also sets the value of Λ [30]. In the absence of such large length scales, however, it was believed that $\Lambda \sim 1/b$, but its precise value would vary by a factor within the entire log-period $e^{\pi/s_0} \approx 22.7$ from one system to another, or even from one Feshbach resonance to another within the same system [31].

However, several recent experiments with identical ultra-cold atoms [2–22] have revealed Efimov trimers and thereby determined their three-body parameters. In these experiments, rather broad Feshbach resonances are used, implying that the range b of the interactions between atoms is typically the van der Waals length $r_{\text{vdW}} = \frac{1}{2}(mC_6/\hbar^2)^{1/4}$ associated with the $-C_6/r^6$ tail of the open-channel potential [29]. The measured value of the three-body parameter expressed in units of r_{vdW} turned out to stay fairly constant for different atomic species [2], nuclear spin states [16], or even different resonances of the same atomic species [18]. This indicates that the three-body parameter is universally determined by the van der Waals length, and relatively insensitive to other short-range details specific to individual atomic species.

It was first suggested that this van der Waals universality was due to the very deep well of the potentials for these species, which support many two-body bound states. According to this conjecture, when the three atoms enter the short-range region of the potential, they feel such a deep potential well that for all these species it results in the same effect on the phase of the wave function, and leads to the same three-body parameter Λ .

However, Efimov features for helium atoms, which interact through a shallow potential supporting only one two-body bound state, were shown to also follow the van der Waals universality, both theoretically [32] and experimentally [22].

A first attempt [33] to explain this universality suggested that it could be due to quantum reflection in the sum of pairwise $-1/r^6$ potentials. Particles coming from large distances to separations on the order of the van der Waals length would experience a sudden drop in the resulting effective three-body potential, which would reflect the particles before they start to probe short-range physics. However, a numerical study [34] showed that the relevant three-body potential in the van der Waals region does not exhibit a sudden drop, but a sudden repulsive barrier. The numerical results indicate that this three-body repulsion is universally located around $R \approx 2r_{\text{vdW}}$ for several model potentials and arises whenever a pairwise interaction potential features a deep well supporting many two-body bound states or a short-range hardcore repulsion, which is the case for all atomic species. Reference [34] attributes the appearance of the repulsive barrier to an increase of kinetic energy due to the squeezing of the hyperangular wave function into a smaller volume caused by the suppression of two-body probability inside the two-body potential well. Reference [35], on the other hand, attributes it to the hard-core repulsion of the two-body potential. It is therefore necessary to clarify how precisely the repulsive barrier emerges, what physical picture it corresponds to, and why it is universal. The purpose of this work is to show that the universality of the three-body parameter indeed originates from the two-body correlation, through a deformation of the three-body system in the van der Waals region.

This paper is organised as follows. In Sec. II, we review how the three-body repulsion setting the three-body parameter arises in the hyperspherical formalism. In Sect. III, we interpret the three-body repulsion as a consequence of three-body deformation induced by pair correlation and show why it is universal. In Sect. IV, we confirm this scenario by using two simple models. In Sect. V, we give the conclusion of this work.

II. THE THREE-BODY REPULSION

The three-body repulsion is observed in the hyperspherical formalism, where the three-body wave function Ψ is expressed in terms of the hyperradius $R = \sqrt{\frac{2}{3}(r_{12}^2 + r_{23}^2 + r_{31}^2)}$, which corresponds to the global size of the three-body system [50], and the hyperangles, which describe the shape of the three-body system and are collectively denoted by Ω . We present here a simple approximation that captures the bare essentials of both the Efi-

mov attraction and the universal three-body repulsion.

The three-body wave function can be expanded over a basis of hyperangular wave functions $\tilde{\Phi}_n(\Omega; R)$ which are normalised to unity:

$$\Psi(R, \Omega) = \frac{1}{R^{5/2}} \sum_n f_n(R) \tilde{\Phi}_n(\Omega; R). \quad (1)$$

The hyperangular wave function $\tilde{\Phi}_n$ itself can be expanded into three Faddeev components $\phi_n^{(i)}$,

$$\tilde{\Phi}_n(\Omega; R) = \sum_{i=1,2,3} \frac{\phi_n^{(i)}(\Omega; R)}{\sin 2\alpha_i}. \quad (2)$$

Here, $\alpha_i = \arctan \frac{\sqrt{3}r_{jk}}{2r_{i,jk}} = \arcsin \frac{r_{jk}}{R}$ is the Delves hyperangle in the i th Jacobi coordinate system $(\vec{r}_{jk}, \vec{r}_{i,jk})$, where (i, j, k) denotes the cyclic permutations of $(1, 2, 3)$. For identical bosons, the functional forms of all Faddeev components are the same, $\phi_n^{(i)} = \phi_n$. The advantage of this Faddeev decomposition is that it treats the three particles on equal footing. In the low-energy Faddeev approximation [36], ϕ_n is assumed to depend only upon the Delves hyperangle α . In this approximation, one ignores the dependence of ϕ_n on the directions of \vec{r}_{jk} and $\vec{r}_{i,jk}$, *i.e.* higher angular momentum partial waves. This excludes the possibility of accidental resonances with higher partial waves [31, 34], and gives less accurate results. Nevertheless, this approximation is good enough for our purpose, as we shall see below.

The Faddeev component ϕ_n is chosen to be the eigen-solution with the eigenvalue λ_n of the Faddeev equation

$$\begin{aligned} & \left(-\frac{\partial^2}{\partial \alpha^2} - \lambda_n \right) \phi_n(\alpha) = \\ & -R^2 \frac{m}{\hbar^2} V(R \sin \alpha) \left(\phi_n(\alpha) + \frac{4}{\sqrt{3}} \int_{\alpha_{\min}}^{\alpha_{\max}} \phi_n(\alpha') d\alpha' \right), \end{aligned} \quad (3)$$

where m is the particle mass, V is the pairwise interaction potential, $\alpha_{\min} = |\frac{\pi}{3} - \alpha|$, and $\alpha_{\max} = \frac{\pi}{2} - |\frac{\pi}{6} - \alpha|$. We assume that three-body interactions are negligible [51].

Each solution ϕ_n defines a channel n , and one finds in general that the hyperradial functions $f_n(R)$ are solutions of the coupled equations,

$$\begin{aligned} & \left(-\frac{\partial^2}{\partial R^2} + \frac{\lambda_p(R)}{R^2} - \frac{1}{4R^2} - \frac{m}{\hbar^2} E \right) f_p(R) \\ & + \sum_n \left(Q_{pn} f_n(R) + 2P_{pn} \frac{\partial f_n(R)}{\partial R} \right) = 0, \end{aligned} \quad (4)$$

with the nonadiabatic couplings

$$Q_{pn} = - \int d\Omega \tilde{\Phi}_p^* \frac{\partial^2 \tilde{\Phi}_n}{\partial R^2}; \quad P_{pn} = - \int d\Omega \tilde{\Phi}_p^* \frac{\partial \tilde{\Phi}_n}{\partial R}. \quad (5)$$

If we restrict our consideration to a particular channel n (neglecting couplings to other channels) and note that

$P_{nn} = 0$ due to the normalisation of $\tilde{\Phi}_n$, we arrive at a simple Schrödinger equation

$$\left(-\frac{\partial^2}{\partial R^2} - \frac{1}{4R^2} + U_n(R) - \frac{m}{\hbar^2}E\right) f_n(R) \approx 0, \quad (6)$$

with the three-body potential

$$U_n(R) = \frac{\lambda_n(R)}{R^2} + Q_{nn}(R). \quad (7)$$

This potential is the sum of adiabatic (first term) and nonadiabatic (second term) contributions. The Efimov attraction manifests itself in this framework as the appearance in a particular channel $n = 0$ of a negative eigenvalue $\lambda_0(R) \rightarrow -s_0^2$ at large hyperradii, with $s_0 \approx 1.00624$. One can show that $Q_{00}(R) \rightarrow O(1/R^3)$, so that the potential $U_0(R)$ tends to the $1/R^2$ Efimov attraction at large R . At shorter distance, the potential becomes repulsive. This is illustrated in Fig. 1, where the three-body potentials $U_n(R)$ obtained by solving Eq. (3) are represented for several two-body potentials with a van der Waals tail. Namely, we used the following soft-core van der Waals and Lennard-Jones potentials,

$$V_{\text{soft}}(r) = -C_6 \frac{1}{r^6 + \sigma^6}, \quad (8)$$

$$V_{\text{LJ}}(r) = C_6 \left(\frac{\sigma^6}{r^{12}} - \frac{1}{r^6} \right), \quad (9)$$

where the length σ is adjusted to produce a shape resonance (divergence of the scattering length, leading to the unitarity limit $a \rightarrow \infty$). There are several possible choices of σ , corresponding to different depths of the potential well, or equivalently different numbers of s -wave two-body bound states n_b (including the one at the breakup threshold). We also use a realistic helium potential [37] rescaled to reach unitarity [32], which is qualitatively similar to a Lennard-Jones potential at unitarity with one two-body bound state.

Figure 1 shows that for all these two-body potentials, the three-body potential $U_0(R)$ in the Efimov channel ($n = 0$) exhibits both the Efimov attraction at large distance and a repulsive barrier at short distance. Consistent with Ref. [34], for all these pairwise potentials with the exception of the soft-core van der Waals potential with one bound state, the repulsive barrier is universally located around $R \approx 2r_{\text{vdW}}$.

III. INTERPRETATION OF THE THREE-BODY REPULSION

A. Repulsion due to deformation

One might think that the repulsive barrier is a consequence of the hard-core repulsion in the two-body potential, as suggested in Ref. [35]. However, this is not the case since it occurs also for the soft van der Waals

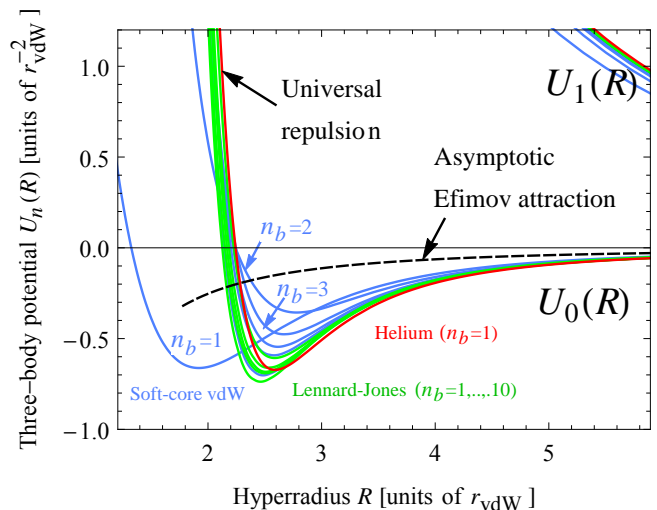


Figure 1: Three-body potentials $U_0(R)$ and $U_1(R)$ for different pairwise interactions at unitarity: soft-core van der Waals potential (blue) with $n_b = 1-10$ two-body bound states, Lennard-Jones potential (green) with $n_b = 1-10$ two-body bound states, and helium potential (red) rescaled to reach unitarity with $n_b = 1$ two-body bound state. Note that only the case of the soft-core van der Waals potential with one bound state is significantly different from the other cases. The dashed curve shows the asymptotic Efimov attraction.

potential which has no repulsive core and is purely attractive. Another counter-intuitive observation is that the depth of the three-body potential U_0 remains relatively stable as the two-body potential is made deeper and deeper. Our calculation shows that the adiabatic contribution $\lambda_0(R)/R^2$ in Eq. (7) gets indeed deeper, but is compensated by the purely repulsive nonadiabatic term Q_{00} . The fact that the nonadiabatic kinetic energy is indeed repulsive at large distance can be understood by rewriting Q_{00} as

$$Q_{00}(R) = \int d\Omega \left| \frac{\partial \tilde{\Phi}_0(\Omega; R)}{\partial R} \right|^2 \geq 0, \quad (10)$$

using the normalisation of $\tilde{\Phi}_0$ and the fact that it can be chosen to be real. This shows that Q_{00} is positive and since it has to vanish at large distance, it must be repulsive (if one excludes unlikely oscillations at infinitely large distance).

Equation (10) shows that the nonadiabatic kinetic energy Q_{00} arises from a change in the hyperangular wave function $\tilde{\Phi}_0$ with respect to the hyperradius, i.e. from a change in the probability distribution of the shape of the three-body system as a function of its size. To visualise this change, we use $\tilde{\Phi}_0$ to plot in Fig. 2 the probability density of finding a particle 3 for a given separation r_{12} of the two other particles 1 and 2,

$$P(\vec{r}_{12,3}) = (\sin 2\alpha_3)^2 \left| \tilde{\Phi}_0(\Omega; R) \right|^2. \quad (11)$$

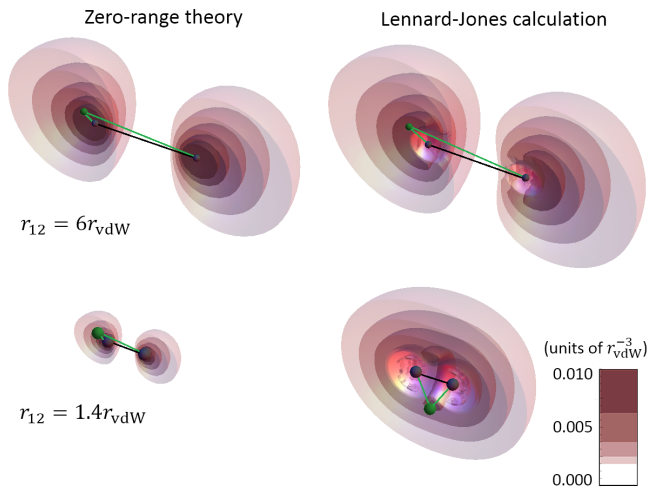


Figure 2: Three-dimensional contour plots of the probability distribution in Eq. (11) of finding a particle for a given separation of the two other particles (which are indicated by a pair of small gray balls connected by a black line). For clarity, we only show the probability density behind a plane containing the two particles, and shade the contours with an opacity increasing with probability density: the darker, the higher the probability of finding the third particle. The top figures correspond to a separation of $6.0 r_{\text{vdW}}$, while the bottom ones correspond to a separation of $1.4 r_{\text{vdW}}$. To appreciate the change in configuration between the figures, a typical location of the third particle is indicated by a small green ball connected to the other two particles by green lines. The left figures were computed from the zero-range Efimov theory at unitarity; they show the invariance of the Efimov configuration distribution with respect to the size of the system. The right figures were computed for a Lennard-Jones pairwise potential at unitarity supporting four two-body bound states. At large separations, the probability distribution is consistent with the Efimov configuration distribution, but around each of the two particles there is a noticeable sphere of radius $\sim r_{\text{vdW}}$ in which the probability is significantly suppressed. This suppression leads to an abrupt change in configuration probability when the particles come close.

When particle 3 is far from particles 1 and 2, the hyperangular wave function is given by the zero-range limit (corresponding to the Efimov theory), which at unitarity admits the following analytical solution [1],

$$\tilde{\Phi}_0^{(\text{ZR})}(\Omega) = \sum_{i=1}^3 \frac{\phi_0^{(\text{ZR})}(\alpha_i)}{\sin 2\alpha_i},$$

with $\phi_0^{(\text{ZR})}(\alpha) = \sinh(s_0(\frac{\pi}{2} - \alpha))$, (12)

which is independent of the hyperradius. The probability density therefore remains the same up to a scale transformation. In other words, the probability distribution of the shape of the three-particle system remains the same, namely the third particle is typically located closer to one of the other two. This invariance of the hyperangular wave function with respect to the hyperradius results in $Q_{00} = 0$.

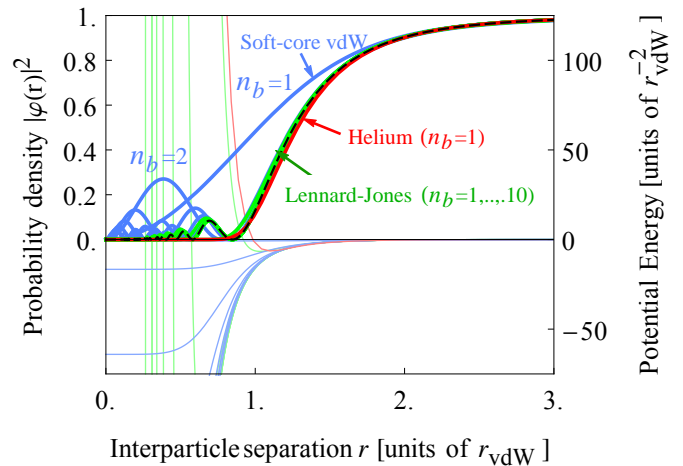


Figure 3: Zero-energy two-body probability density distribution $|\varphi|^2$ (normalised asymptotically to unity) as a function of interparticle distance for different two-body potentials: soft-core van der Waals potential (blue) with $n_b = 1-8$ bound states, Lennard-Jones potential (green) with $n_b = 1-8$ bound states, helium potential (red) rescaled to reach unitarity with one bound state. The corresponding potentials are shown in faded colours. The probability density corresponding to the universal van der Waals correlation given in Eq. (13) is shown by the dashed black curve.

When particle 3 comes close to particle 1 or 2, however, this zero-range picture becomes invalid because the finite-range effects of the interaction are no longer negligible. In Fig. 2, one can clearly see two regions of suppressed probability near particles 1 and 2. This exclusion is an expected consequence of the known two-body physics. It is expected indeed that for short-range interactions the three-body density distribution becomes proportional to the relative two-body density distribution whenever two particles come sufficiently close, as recently illustrated in nuclear physics [38]. The relative radial probability density distribution $|\varphi|^2$ for two particles at zero scattering energy is represented in Fig. 3 for different two-body potentials at unitarity. One can see that the probability is indeed suppressed below some radius on the order of r_{vdW} due to either the presence of a repulsive wall or, on the contrary, the acceleration in the well of the potential.

As particles 1 and 2 come close, this two-body exclusion confines the probability distribution for particle 3 to a region forming a ring in between the two particles, corresponding to an equilateral shape of the three-particle system. We find that this change of shape happens very suddenly, making it difficult for the system to follow the Efimov channel adiabatically (see the the supplementary materials for the animations corresponding to the left side (zero-range theory) and right side (Lennard-Jones calculations) of Fig. 2). This abrupt variation results in a significant gain of nonadiabatic kinetic energy Q_{00} in Eq. (10), thereby creating the three-body repulsion. In light of this discussion, we expect the three-body repulsion to be essentially determined by the form of the pair

correlation.

B. van der Waals universality

The pair correlation for two particles interacting with van der Waals interactions is known to have a universal asymptotic form [39, 40]. In particular, the zero-energy radial two-body wave function φ for a given scattering length a has the following analytical form in the van der Waals tail region:

$$\varphi(r) = \Gamma(5/4)\sqrt{x}J_{1/4}(2x^{-2}) - \frac{r_{\text{vdW}}}{a}\Gamma(3/4)\sqrt{x}J_{-1/4}(2x^{-2}), \quad (13)$$

where Γ and J_α denote the gamma and Bessel functions, and $x = \frac{r}{r_{\text{vdW}}}$. At large distance, $\varphi(r)$ asymptotes to the free wave form $1 - \frac{r}{a}$. For $a \rightarrow \infty$, $\varphi(r)$ asymptotes to unity and thus can be regarded as a correlation function describing the deviations from the free wave. The corresponding two-body probability density $|\varphi|^2$ is represented in Fig. 3 by the black dashed curve. One can see that the probability densities obtained for all the considered potentials nearly coincide with this analytical form for $r \gtrsim r_{\text{vdW}}$. For potentials which strongly suppress the probability for $r \lesssim r_{\text{vdW}}$, the whole pair correlation is thus very similar to the universal correlation. This similarity holds even for shallow potentials with a short van der Waals tail accompanied by a hard-core repulsion, such as that of helium. The fact that the short-distance oscillations of the universal correlation are not reproduced does not make any major difference, because the probability density is very small in this region. Since the two-body correlation is nearly the same for these potentials, the same nonadiabatic deformation occurs, leading to the same three-body repulsion and three-body parameter. Conversely, the soft-core van der Waals potential with one two-body bound state leads to a pair correlation that deviates from the universal correlation more significantly, with a less pronounced suppression of probability, as seen in Fig. 3. According to our interpretation, this should create a softer three-body repulsion at a shorter hyperradius. This is indeed the case, as can be checked in Fig. 1.

In the present interpretation, the universality of the three-body parameter is thus a direct consequence of the van der Waals two-body correlation.

IV. CHECK WITH SIMPLE MODELS

To verify our interpretation, we construct two simple models. The first one verifies that the pair correlation does indeed create a three-body repulsive barrier at $R \approx 2r_{\text{vdW}}$ in the Efimov channel through the nonadiabatic kinetic energy. The second one is a more complete model verifying quantitatively that the pair correlation

fixes the three-body parameter to a value consistent with full numerical calculations and experiments.

A. Pair correlation model

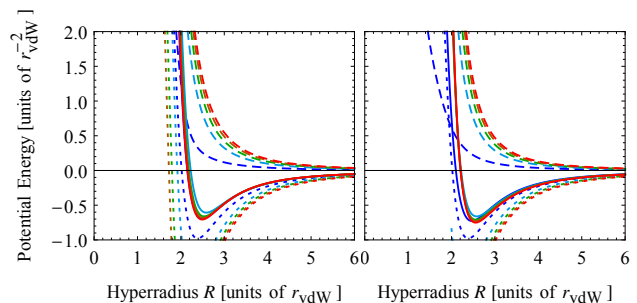


Figure 4: Comparison between the Faddeev three-body calculations (left) and the simple two-body correlation model described in the main text (right). The dashed curves show the nonadiabatic kinetic energy Q_{00} for Lennard-Jones potentials of different depths, corresponding to the unitarity limit with different numbers of two-body bound states ranging from 1 to 5. The solid curves show the full three-body potential $U_0(R)$ obtained by adding to Q_{00} the adiabatic contribution λ_0/R^2 obtained from Faddeev calculations, which is shown by the dotted curves.

To simply account for the two-body suppression, we consider a trial hyperangular wave function of the Bijl-Jastrow form [41, 42], which is the uncorrelated hyperangular function $\tilde{\Phi}_0^{(\text{ZR})}$ in the zero-range (Efimov) limit given by Eq. (12), multiplied by a product of the universal two-body correlation φ given by Eq. (13), which causes the suppression of probability in the two-body sector:

$$\tilde{\Phi}_0^{(\text{model})} = \tilde{\Phi}_0^{(\text{ZR})} \times \prod_{i < j} \varphi(r_{ij}). \quad (14)$$

This simple ansatz leads to a probability density that is very similar to the one calculated from the Faddeev equation (3). In particular, we have confirmed that it also leads to a sudden buildup of probability in the ring-shaped region when two particles are close. One can also calculate the nonadiabatic kinetic energy Q_{00} from Eq. (10). As expected, we find a sudden increase of Q_{00} at the hyperradius $R \approx 2r_{\text{vdW}}$. This model thus confirms our claim that the nonadiabatic change in configuration originates from an interplay between the suppression of two-body probability and the Efimov configuration.

Adding the adiabatic term $\frac{\lambda_0}{R^2}$ to Q_{00} , we obtain the full potential $U_0(R)$. As shown in Fig. 4, it reproduces very well the universal potential found using the solution of the Faddeev equation (3). Note that this agreement is remarkable; although the adiabatic and nonadiabatic terms taken separately vary significantly for different numbers of two-body bound states, their variations almost cancel out to give the universal potential.

B. Separable model

The hyperspherical formalism is useful to exhibit the three-body repulsion mechanism, and the previous model satisfactorily reproduces the three-body repulsion in the Efimov channel. However, this channel alone only gives qualitative results for the actual trimer energies. To be more quantitative, one would need to solve the many coupled equations in Eq. (4), as done in Ref. [34], but that would defeat our purpose of using a simple model to reproduce the physics. Hence we turn to another approach to get more quantitative results, while keeping the central idea of the universal pair correlation in Eq. (13) being the essential ingredient behind the universal three-body parameter.

One of the simplest pseudo-potentials that can reproduce the universal pair correlation is the separable potential [43, 44],

$$\hat{V} = \frac{\hbar^2}{m} \xi |\chi\rangle\langle\chi|, \quad (15)$$

where the function χ in momentum space is chosen to be

$$\chi(q) = 1 - q \int_0^\infty dr \left(1 - \frac{r}{a} - \varphi(r)\right) \sin(qr), \quad (16)$$

and the coefficient ξ is set to

$$\xi = 4\pi \left(\frac{1}{a} - \frac{2}{\pi} \int_0^\infty dq |\chi(q)|^2 \right)^{-1}. \quad (17)$$

This potential has the advantage of being easily tractable because of its separability, and one can show (see Appendix B) that the solution of the two-body problem at zero energy for this potential is given exactly by $\varphi(r)$, which is chosen to be the universal pair correlation given by Eq. (13). Numerically, we find that this potential is an excellent substitute for the real van der Waals interaction in the two-body problem at low energy: it reproduces the low-energy scattering state and the two-body bound state over energies on the order of $\hbar^2/(mr_{\text{vdW}}^2)$ and scattering lengths $|a| \gtrsim 2r_{\text{vdW}}$.

For the three-body problem, substituting the real potential by the separable potential in the three-body Schrödinger equation leads to a one-dimensional integral equation [45, 46] that is similar to the Skorniakov–Ter-Martirosian equation obtained for a contact potential [47] and that can easily be solved numerically (see the Appendix B for the derivation). We emphasise that the only information contained in this model is the zero-energy pair correlation.

From the numerical solution, we obtain the ground-state trimer spectrum shown in Fig. 5. In particular, we extract the binding wave number κ at unitarity and the scattering length a_- at which this trimer disappears in the three-body threshold, and find

$$\kappa r_{\text{vdW}} = 0.187(1) \quad \text{and} \quad \frac{a_-}{r_{\text{vdW}}} = -10.86(1).$$

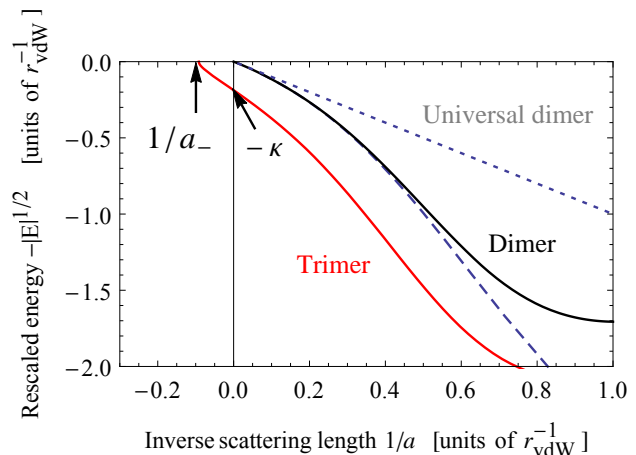


Figure 5: Lowest trimer and dimer energy for the separable potential given by Eq. (15), as a function of its inverse scattering length $1/a$. For comparison, the dotted and dashed curves represent the universal dimer energy ($E = -\frac{\hbar^2}{ma^2}$) and the exact van der Waals dimer energy, respectively. Both the abscissa and ordinate are shown in units of the inverse van der Waals length r_{vdW}^{-1} .

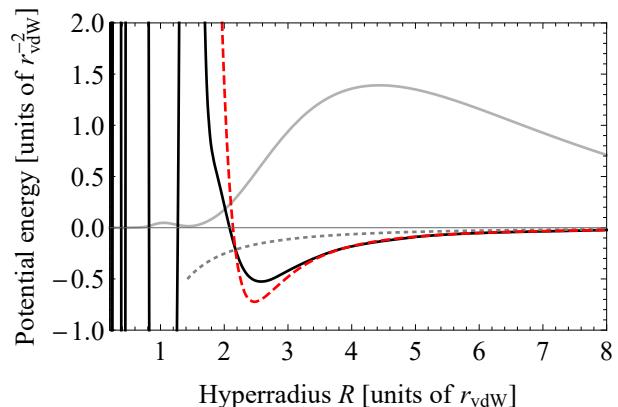


Figure 6: Three-body probability (solid gray curve, in arbitrary units) as a function of hyperradius, and corresponding effective three-body potential (solid black curve), obtained from the separable model Eq. (15). For comparison, the Efimov potential (dotted curve) and the low-energy Faddeev three-body potential obtained from Eq. (7) for a Lennard-Jones potential with six s-wave bound states (red dashed curve) are also represented. Note that for $R < 1.5r_{\text{vdW}}$, the effective potential becomes strongly oscillatory (as can be seen from the nearly vertical lines) in order to reproduce the wave function. Since the physics in that region is correctly described by coupled potentials, the effective potential is not a meaningful construct in that region and the short-range oscillations have no particular significance.

Consistent with our interpretation, similar results are obtained for pair correlations $\varphi(r)$ with a similar tail and low probability at short distance. For instance, the pair correlation for a Lennard-Jones potential with one two-

body bound state leads to $\kappa r_{\text{vdW}} = 0.205(1)$ and $\frac{a_-}{r_{\text{vdW}}} = -10.23(1)$. These values agree within a few percent with the results of [34], and are in fair agreement with the experimental result of $\frac{a_-}{r_{\text{vdW}}} = -9.1(5)$ [48].

Finally, one can check that this agreement is not coincidental, as the model also reproduces the deformation and repulsion effects. This is demonstrated by the three-body probability plotted as a function of R in Fig. 6. By calculating the second-order derivative of the corresponding wave function, one can derive an effective hyperradial potential (see Appendix C). This potential reproduces very closely the three-body potential calculated from the low-energy Faddeev equation. Only the repulsive barrier is slightly shifted to a smaller hyperradius, resulting in a more quantitatively accurate three-body parameter.

V. CONCLUSION

We have shown that the universality of the three-body parameter revealed in recent experiments with neutral atoms and numerical calculations originates from two-body correlation.

The mechanism explaining this origin is the following: two-body correlation suppresses the probability for two atoms to be at separations smaller than the van der Waals length, which imposes a deformation of the three-atom system when the three atoms come within the distance of the van der Waals length. The kinetic-energy cost associated with this deformation creates a repulsion preventing the three atoms from coming closer, and sets the three-body parameter.

This mechanism is consistent with the findings of J. Wang *et al.* [34]. Unlike other proposed mechanisms [33, 35], this does not necessitate a hard-core repulsion in the two-body potential, nor is it simply the expression of quantum reflection along a single coordinate since it involves the three-body deformational degrees of freedom.

Because the two-body correlation is universally determined by the van der Waals length for atomic systems, this makes the three-body parameter universal in these systems. More generally, we expect to find such universality in any class of systems where the two-body suppression has a universal form. This work also suggests that for other systems, in general, pair correlations and their associated length scale, the effective range, should play an essential role. These points are addressed in more detail in a separate paper [49].

We thank C. Greene for suggesting the plot in Fig. 6 and Ch. Elster for making us aware of Ref. [44]. P. N. acknowledges support from RIKEN through the Incentive Research Project funding. S. E. acknowledges support from JSPS. M. U. and P. N. acknowledge the hospitality of the Aspen Center for Physics where part of this work was done. M. U. acknowledges the financial support from Grants-in-Aid (KAKENHI Grant Nos.

26287088 and 22103005) and the Photon Frontier Network Program from MEXT of Japan.

Appendix A

In this Appendix, we show that the radial wave function φ in Eq. (16) is the solution of the two-body problem at zero energy for the separable potential given by Eq. (15). A more general representation of two-body interactions in terms of separable potentials can be found in Ref. [44].

The two-body Schrödinger equation at zero energy in momentum space reads:

$$\frac{\hbar^2 p^2}{m} \tilde{\psi}(\vec{p}) + \int \frac{d^3 \vec{q}}{(2\pi)^3} \tilde{V}(\vec{p}, \vec{q}) \tilde{\psi}(\vec{q}) = 0, \quad (18)$$

where \tilde{V} is the Fourier transform of the pairwise potential V , and $\tilde{\psi}$ is the Fourier transform of the two-body wave function. Replacing \tilde{V} by the separable potential in Eq. (15), one obtains:

$$p^2 \tilde{\psi}(\vec{p}) - f \chi(p) = 0, \quad (19)$$

with

$$f = - \int \frac{q^2 dq}{2\pi^2} \tilde{\psi}(\vec{q}) \xi \chi^*(q). \quad (20)$$

Inserting Eq. (19) into Eq. (20), one obtains the explicit expression for f :

$$f = - \left(\frac{1}{\xi} + \int \frac{dq}{2\pi^2} |\chi(q)|^2 \right)^{-1}, \quad (21)$$

and using the chosen form of ξ given by Eq. (17), one obtains $f = -4\pi a$. Inserting this value into Eq. (19), and inverting the resulting equation with the proper boundary conditions, one finds:

$$\tilde{\psi}(\vec{p}) = (2\pi)^3 \delta^3(\vec{p}) - 4\pi a \frac{\chi(p)}{p^2}. \quad (22)$$

This translates in space coordinates as

$$\psi(\vec{r}) = 1 - 4\pi a \int \frac{d^3 p}{(2\pi)^3} \frac{\chi(p)}{p^2} e^{i\vec{p}\cdot\vec{r}}, \quad (23)$$

which after angular integration yields:

$$\psi(\vec{r}) = 1 - a \frac{2}{\pi} \int_0^\infty \chi(p) \frac{\sin pr}{pr} dp. \quad (24)$$

Inserting the chosen form of χ given by Eq. (16), and using the closure relation $\int_0^\infty dp \sin(pr') \sin(pr) = \frac{\pi}{2} \delta(r - r')$, one obtains

$$\psi(\vec{r}) = -\frac{a}{r} \varphi(r), \quad (25)$$

which shows that the form of the zero-energy radial wave function $r\psi(\vec{r})$ is indeed given by $\varphi(r)$.

Appendix B

In this Appendix, we derive the equation we use to solve the three-body problem with the separable potential given by Eq. (15).

The three-body Schrödinger equation in momentum space reads:

$$\left(\frac{3}{4}\frac{\hbar^2}{m}P^2 + \frac{\hbar^2}{m}p^2 - E\right)\tilde{\Psi}(\vec{P}, \vec{p}) + \sum_{i=1,2,3} \int \frac{d^3\vec{q}_i}{(2\pi)^3} \tilde{V}(\vec{p}_i, \vec{q}_i)\tilde{\Psi}(\vec{P}_i, \vec{q}_i) = 0, \quad (26)$$

where \tilde{V} is the Fourier transform of the pairwise potential V , and $\tilde{\Psi}$ is the Fourier transform of the three-body wave function Ψ in Eq. (1) expressed in a particular Jacobi coordinate set (\vec{P}, \vec{p}) chosen among the three possible sets (\vec{P}_i, \vec{p}_i) with $i = 1, 2, 3$.

Substituting \tilde{V} by the separable potential in Eq. (15), one obtains:

$$\left(\frac{3}{4}P^2 + p^2 - \frac{m}{\hbar^2}E\right)\tilde{\Psi}(\vec{P}, \vec{p}) + \sum_{i=1,2,3} F(\vec{P}_i)\chi(p_i) = 0, \quad (27)$$

where

$$F(\vec{P}) = \xi \int \frac{d^3\vec{p}}{(2\pi)^3} \chi^*(p)\tilde{\Psi}(\vec{P}, \vec{p}). \quad (28)$$

For $E < 0$, Eq. (27) can be inverted as

$$\tilde{\Psi}(\vec{P}, \vec{p}) = - \sum_{i=1,2,3} \frac{F(\vec{P}_i)\chi(p_i)}{\frac{3}{4}P^2 + p^2 - \frac{m}{\hbar^2}E}, \quad (29)$$

Inserting Eq. (29) into Eq. (28) gives:

$$\frac{1}{\xi}F(\vec{P}) = - \sum_{i=1,2,3} \int \frac{d^3\vec{p}}{(2\pi)^3} \chi^*(p) \frac{F(\vec{P}_i)\chi(p_i)}{\frac{3}{4}P^2 + p^2 - \frac{m}{\hbar^2}E}. \quad (30)$$

Making the choice $(\vec{P}, \vec{p}) = (\vec{P}_3, \vec{p}_3)$, one can factorise one of the terms in the sum with the left-hand side of Eq. (30) as follows:

$$\left(\frac{1}{\xi} + \int \frac{d^3\vec{p}}{(2\pi)^3} \frac{|\chi(p)|^2}{\frac{3}{4}P^2 + p^2 - \frac{m}{\hbar^2}E}\right)F(\vec{P}) + \sum_{i=1,2} \int \frac{d^3\vec{p}}{(2\pi)^3} \chi^*(p) \frac{F(\vec{P}_i)\chi(p_i)}{\frac{3}{4}P^2 + p^2 - \frac{m}{\hbar^2}E} = 0. \quad (31)$$

The two remaining terms are equal due to bosonic exchange symmetry, and expressing one Jacobi coordinate set in terms of another, one finally arrives at the integral equation for F :

$$\left(\frac{1}{\xi} + \int \frac{d^3\vec{q}}{(2\pi)^3} \frac{|\chi(q)|^2}{q^2 - (\frac{mE}{\hbar^2} - \frac{3}{4}P^2)}\right)F(\vec{P}) + 2 \int \frac{d^3\vec{q}}{(2\pi)^3} \frac{\chi^*(|\vec{q} + \frac{\vec{P}}{2}|)\chi(|\frac{\vec{q}}{2} + \vec{P}|)}{P^2 + q^2 + \vec{q} \cdot \vec{P} - \frac{mE}{\hbar^2}}F(\vec{q}) = 0. \quad (32)$$

For spherically-symmetric solutions, it can be reduced to an equation in which F depends only on the one-dimensional variable $P = |\vec{P}|$:

$$D(P)F(P) + \int_0^\infty \frac{q^2 dq}{2\pi^2} H(P, q)F(q) = 0, \quad (33)$$

with

$$D(P) = \frac{1}{\xi} + \int_0^\infty \frac{dq}{2\pi^2} \frac{q^2 |\chi(q)|^2}{q^2 - (\frac{mE}{\hbar^2} - \frac{3}{4}P^2)}, \quad (34)$$

$$H(P, q) = \int_{-1}^1 du \frac{\chi^*(\sqrt{q^2 + \frac{1}{4}P^2 + qPu})\chi(\sqrt{P^2 + \frac{1}{4}q^2 + qPu})}{P^2 + q^2 + qPu - \frac{mE}{\hbar^2}}. \quad (35)$$

Solving for the eigenvalues of the linear operator in the left-hand side of Eq. (33) and looking for the energies E that make one of these eigenvalues equal to zero, consistent with the right-hand side of Eq. (33), yields the energies of three-body bound states. The corresponding eigenvectors F give the three-body wave functions Ψ through Eq. (29).

Appendix C

The explicit procedure to calculate the effective hyper-radial potential (black curve of Fig. 7) is the following.

First, the form of the Faddeev components in hyperspherical coordinates is calculated from the solution $F(P)$ of Eq. (33) in Appendix B:

$$\mathcal{F}(R, \alpha) = \frac{-4}{\sqrt{3}R^2 \sin 2\alpha} \int \int \frac{PdP p dp}{2\pi^2 2\pi^2} \frac{F(P)\chi(p)}{\frac{3}{4}P^2 + p^2 - \frac{m}{\hbar^2}E} \times \sin\left(P\frac{\sqrt{3}}{2}R \cos \alpha\right) \sin(pR \sin \alpha). \quad (36)$$

The total wave function is thus

$$\Psi(R, \alpha) = \mathcal{F}(R, \alpha_3) + \mathcal{F}(R, \alpha_2) + \mathcal{F}(R, \alpha_1) \quad (37)$$

with

$$\alpha_3 = \alpha, \quad (38)$$

$$\alpha_2 = \frac{1}{2} \left(\pi - \arccos \left(\frac{1}{2} \cos 2\alpha - u \frac{\sqrt{3}}{2} \sin 2\alpha \right) \right), \quad (39)$$

$$\alpha_1 = \frac{1}{2} \left(\pi - \arccos \left(\frac{1}{2} \cos 2\alpha + u \frac{\sqrt{3}}{2} \sin 2\alpha \right) \right), \quad (40)$$

where u is the cosine of the angle between the two Jacobi vectors \vec{r}_{12} and $\vec{r}_{3,12}$. The hyper-radial density (grey curve of Fig. 7) is therefore given by:

$$\rho(\mathcal{R}) \propto R^5 \int_{-1}^1 du \int_0^{\pi/2} \sin^2 2\alpha |\Psi(R, \alpha)|^2. \quad (41)$$

Interpreting this density as an effective hyperradial wave function $f(R) = \sqrt{\rho(R)}$ satisfying a Schrödinger equation similar to Eq. (6) for an uncoupled potential $U_{\text{eff}}(R)$, one finds:

$$U_{\text{eff}}(R) = \frac{1}{4R^2} + \frac{f''(R)}{f(R)} + \frac{m}{\hbar^2} E. \quad (42)$$

-
- [1] V. Efimov, *Sov. J. Nucl. Phys.* **12**, 589 (1971).
[2] F. Ferlaino and R. Grimm, *Physics* **3**, 9 (2010).
[3] T. Kraemer, M. Mark, P. Waldburger, J. G. A. Danzl, C. Chin, B. Engeser, A. Lange, K. Pilch, A. Jaakkola, H. Nägerl, et al., *Nature* **440**, 315 (2006).
[4] T. B. Ottenstein, T. Lompe, M. Kohnen, A. N. Wenz, and S. Jochim, *Phys. Rev. Lett.* **101**, 203202 (2008).
[5] J. H. Huckans, J. R. Williams, E. L. Hazlett, R. W. Stites, and K. M. O'Hara, *Phys. Rev. Lett.* **102**, 165302 (2009).
[6] J. R. Williams, E. L. Hazlett, J. H. Huckans, R. W. Stites, Y. Zhang, and K. M. O'Hara, *Phys. Rev. Lett.* **103**, 130404 (2009).
[7] M. Zaccanti, B. Deissler, C. D'Errico, M. Fattori, M. Jona-Lasinio, S. Müller, G. Roati, and G. M. M. Inguscio, *Nature Physics* **5**, 586 (2009).
[8] G. Barontini, C. Weber, F. Rabatti, J. Catani, G. Thalhammer, M. Inguscio, and F. Minardi, *Phys. Rev. Lett.* **103**, 043201 (2009).
[9] A. N. Wenz, T. Lompe, T. B. Ottenstein, F. Serwane, G. Zürn, and S. Jochim, *Phys. Rev. A* **80**, 040702 (2009).
[10] S. E. Pollack, D. Dries, and R. G. Hulet, *Science* **326**, 1683 (2009).
[11] N. Gross, Z. Shotan, S. Kokkelmans, and L. Khaykovich, *Phys. Rev. Lett.* **103**, 163202 (2009).
[12] S. Knoop, F. Ferlaino, M. Mark, M. Berninger, H. Schoebel, H.-C. Nägerl, and R. Grimm, *Nature Physics* **5**, 227 (2009).
[13] T. Lompe, T. B. Ottenstein, F. Serwane, K. Viering, A. N. Wenz, G. Zürn, and S. Jochim, *Phys. Rev. Lett.* **105**, 103201 (2010).
[14] T. Lompe, T. B. Ottenstein, F. Serwane, A. N. Wenz, G. Zürn, and S. Jochim, *Science* **330**, 940 (2010).
[15] S. Nakajima, M. Horikoshi, T. Mukaiyama, P. Naidon, and M. Ueda, *Phys. Rev. Lett.* **105**, 023201 (2010).
[16] N. Gross, Z. Shotan, S. Kokkelmans, and L. Khaykovich, *Phys. Rev. Lett.* **105**, 103203 (2010).
[17] S. Nakajima, M. Horikoshi, T. Mukaiyama, P. Naidon, and M. Ueda, *Phys. Rev. Lett.* **106**, 143201 (2011).
[18] M. Berninger, A. Zenesini, B. Huang, W. Harm, H.-C. Nägerl, F. Ferlaino, R. Grimm, P. S. Julienne, and J. M. Hutson, *Phys. Rev. Lett.* **107**, 120401 (2011).
[19] F. Ferlaino, S. Knoop, M. Berninger, W. Harm, J. P. D'Incao, H.-C. Nägerl, and R. Grimm, *Phys. Rev. Lett.* **102**, 140401 (2009).
[20] O. Machtey, Z. Shotan, N. Gross, and L. Khaykovich, *Phys. Rev. Lett.* **108**, 210406 (2012).
[21] A. Zenesini, B. Huang, M. Berninger, S. Besler, H.-C. Nägerl, F. Ferlaino, R. Grimm, C. H. Greene, and J. von Stecher, *New J. Phys.* **15**, 043040 (2013).
[22] S. Knoop, J. S. Borbely, W. Vassen, and S. J. J. M. F. Kokkelmans, *Phys. Rev. A* **86**, 062705 (2012).
[23] D. S. Petrov, *Phys. Rev. Lett.* **93**, 143201 (2004).
[24] E. Braaten and H.-W. Hammer, *Annals of Physics* **322**, 120 (2007).
[25] M. T. Yamashita, L. Tomio, A. Delfino, and T. Frederico, *Europhys. Lett.* **75**, 555 (2006).
[26] H.-W. Hammer and L. Platter, *Eur. Phys. J. A* **32**, 113 (2007).
[27] J. von Stecher, J. P. D'Incao, and C. H. Greene, *Nature Physics* **5**, 417 (2009).
[28] K. G. Wilson, *Phys. Rev. D* **3**, 1818 (1971).
[29] C. Chin, R. Grimm, P. S. Julienne, and E. Tiesinga, *Rev. Mod. Phys.* **82**, 1225 (2010).
[30] Y. Wang, J. P. D'Incao, and C. H. Greene, *Phys. Rev. Lett.* **106**, 233201 (2011).
[31] J. P. D'Incao, C. H. Greene, and B. D. Esry, *J. Phys. B* **42**, 044016 (2009).
[32] P. Naidon, E. Hiyama, and M. Ueda, *Phys. Rev. A* **86**, 012502 (2012).
[33] C. Chin (2011), [arXiv:1111.1484](https://arxiv.org/abs/1111.1484).
[34] J. Wang, J. P. D'Incao, B. D. Esry, and C. H. Greene, *Phys. Rev. Lett.* **108**, 263001 (2012).
[35] P. K. Sørensen, D. V. Fedorov, A. S. Jensen, and N. T. Zinner, *Phys. Rev. A* **86**, 052516 (2012).
[36] D. V. Fedorov and A. S. Jensen, *Phys. Rev. Lett.* **71**, 4103 (1993).
[37] R. A. Aziz and M. J. Slaman, *J. Chem. Phys.* **94**, 8047 (1991).
[38] M. Alvioli, C. Ciofi degli Atti, L. P. Kaptari, C. B. Mezzetti, H. Morita, and S. Scopetta, *Phys. Rev. C* **85**, 021001(R) (2012).
[39] B. Gao, *Phys. Rev. A* **58**, 4222 (1998).
[40] V. V. Flambaum, G. F. Gribakin, and C. Harabati, *Phys. Rev. A* **59**, 1998 (1999).
[41] A. Bijl, *Physica* **7**, 869 (1940).
[42] R. Jastrow, *Phys. Rev.* **98**, 1479 (1955).
[43] Y. Yamaguchi, *Phys. Rev.* **95**, 1628 (1954).
[44] D. J. Ernst, C. M. Shakin, and R. M. Thaler, *Phys. Rev. C* **8**, 46 (1973).
[45] M. D. Lee, T. Köhler, and P. S. Julienne, *Phys. Rev. A* **76**, 012720 (2007).
[46] P. Naidon and M. Ueda, *Comptes Rendus Physique* **12**, 13 (2011).
[47] G. Skorniakov and K. Ter-Martirosian, *Sov. Phys. JETP* **4**, 648 (1957).
[48] F. Ferlaino, A. Zenesini, M. Berninger, B. Huang, H.-C. Nägerl, and R. Grimm, *Few-Body Syst.* **51**, 113 (2011).
[49] P. Naidon, S. Endo, and M. Ueda, *Phys. Rev. Lett.* **112**, 105301 (2014).
[50] There are several conventions for the definition of the hyperradius. We choose the definition of Ref. [1], which differs by a factor $\sqrt{\sqrt{3}/2} \approx 0.93$ from that of Ref. [34]

for the case of three identical bosons.

[51] This is justified to the extent that the range of the physical three-body force does not exceed the range of the

three-body repulsion.